Journal of Electric Propulsion

RESEARCH Open Access

Resolving multi-dimensional plasma phenomena in Hall thrusters using the reduced-order particle-in-cell scheme

Maryam Reza*, Farbod Faraji* and Aaron Knoll*

*Correspondence:
m.reza20@imperial.ac.uk;
f.faraji20@imperial.ac.uk;
a.knoll@imperial.ac.uk

Department of Aeronautics, Plasma Propulsion Laboratory, Imperial College London, Exhibition Road, London SW7 2AZ, UK

Abstract

Plasma in Hall thrusters exhibits a complex behavior, characterized by the interplay between various dominant processes in each of the thruster's coordinates. The emergence of high-power Hall thrusters in the recent years and the design modifications intended to extend the lifetime of these devices have further amplified the three-dimensional nature of the plasma behavior. In this regard, the novel reduced-order particle-in-cell (PIC) scheme provides the possibility to resolve the multi-dimensional interactions in a Hall thruster at a computational cost up to two orders of magnitude lower than current multi-dimensional PIC simulations. To demonstrate this point, we present in this article the results from a series of pseudo-two-dimensional simulations we performed in three configurations: axial-azimuthal, azimuthal-radial, and axial-radial. We show that, in each configuration, the pseudo-2D PIC scheme provides a significantly improved picture of the involved physics compared to a one-dimensional PIC simulation and captures self-consistently the coupling between the plasma processes in different directions, notably similar to the observations from full-2D kinetic simulations.

Keywords: Hall thruster, Multi-dimensional phenomena, Azimuthal instabilities, Plasma-wall interactions, Particle-in-cell simulation, Reduced-order scheme

Introduction

Since their first appearance in the 1960s, numerous designs of Hall thrusters across the power and size spectrum have emerged, and the technology has steadily become more mature. Today, Hall thrusters of very high input-power and throughput capability are undergoing the late-stage development and qualification campaigns for the next-generation space missions, from on-orbit servicing to manned missions to the Moon and Mars. Nonetheless, several decades of development and research into the Hall thruster technology have revealed the complex underlying physics of operation of these devices [1]. The behavior of plasma in a Hall thruster is governed by a multitude of inter-related, multi-dimensional phenomena that extend across a wide range of spatial and temporal scales [1, 2]. These phenomena and their interactions strongly influence the performance, stability and lifetime of Hall thrusters [3, 4].

Plasma instabilities and turbulence, arising due to strong anisotropy and gradients in the plasma properties, are among the main processes that can notably affect the operation of Hall thrusters. The characteristics of these instabilities are a strong function of the operating condition. Moreover, their evolution dynamics is affected by coupling to the near-wall processes, such as the Secondary Electron Emission (SEE) [5], and by the bulk-plasma processes, such as the electron-neutral collisions [6]. Moreover, there is increasing evidence pointing to the coupling between various instability modes in the Hall thruster's plasma [7]. The impact of plasma instabilities and turbulence on Hall thrusters' operation can be overall divided into two main categories: (1) electrons' cross-field transport [8], and (2) the heating of the plasma species [9].

Plasma interactions with the channel walls of Hall thrusters also play a major role in determining the global plasma behavior by establishing a coupling between the near-wall and bulk plasma processes [1]. The dynamic behavior of the plasma sheath and the variations in the SEE regime, particularly in the presence of the plasma turbulence, is observed to notably influence the electrons' dynamics [5] and, consequently, the associated processes such as the ionization, ion acceleration, and instabilities' evolution.

According to the above overview, it is clear that the plasma behavior is intrinsically three-dimensional in Hall thrusters and is, perhaps, more so in the advanced thrusters in development today that feature unconventional magnetic field topologies. Therefore, from a scientific perspective, a comprehensive picture of the underlying physics can only be acquired using 3D self-consistent kinetic simulations. In addition, from an engineering point of view, noting the significant effects that the multi-dimensional plasma processes in Hall thrusters have on their operation, the ability to predict the evolution of these processes using reliable, self-consistent numerical models can majorly aid the development and testing of advanced Hall thrusters, yielding notable savings in terms of cost and time, and mitigating the potential technical risks associated with these new technologies.

High-fidelity kinetic particle-in-cell (PIC) simulations are optimal tools to investigate in detail the particles' dynamics and interactions in a Hall thruster. However, being a 3D PIC simulation currently unfeasible due to limitations in the available computational resources, lower dimensionality PIC simulations in various two-dimensional configurations have been employed with the hope of untangling the complex nature of the involved physical processes in Hall thrusters. This practice has resulted in numerous insights into the physics of Hall thruster's operation [1, 2]. Nonetheless, the attempts to translate these insights into generalizable closure models to enable predictive, computationally efficient numerical tools has not been yet fully successful. Moreover, the computational cost of traditional multi-dimensional PIC codes can be so enormous for full-scale Hall thrusters that their direct application as a predictive design and test-aiding tool is currently impractical.

With the aim of leveraging the great benefits of the PIC simulations and to mitigate their computational cost, we introduced in a previous publication [10] a novel particle-in-cell scheme, which is based on splitting the two-dimensional Poisson's equation into a system of 1D equations, yielding a reduced-order "pseudo-2D" description of the problem. It is noteworthy that other efforts have been also initiated recently in the community to tackle the computational cost issue of kinetic plasma simulations through

devising an alternative PIC scheme based on the sparse grid techniques [11]. Nevertheless, in Ref. [10], through an extensive study and sensitivity analysis, we demonstrated the great potentials of the pseudo-2D approach in an axial-azimuthal Hall thruster simulation setup. Based on the obtained results, we highlighted that the "pseudo-2D" PIC scheme serves as a strong foundation to progress toward achieving 3D approximations of the Hall thruster plasma. It was additionally emphasized in Ref. [10] that the mathematical formulation behind the decomposition of Poisson's equation in the pseudo-2D PIC scheme is not yet mature and the work is ongoing to address this shortcoming.

Nevertheless, the remarkable accuracy of the predictions of the pseudo-2D scheme in the axial-azimuthal coordinates, even with its preliminary underpinning formulation, prompted us to evaluate the applicability of the pseudo-2D PIC scheme to study multi-dimensional plasma processes in Hall thrusters. The two main questions that we intended to answer were: (1) to what extent the pseudo-2D PIC scheme is capable of capturing the coupling between the plasma processes along the different coordinates in a Hall thruster, and (2) whether resolving an average effect of the radial and azimuthal physical mechanisms is sufficient to obtain a reasonably accurate prediction of the axial distribution of the macroscopic plasma properties.

To present the answers to the two questions posed above, we start in "IPPL particle-in-cell code and the pseudo-2D PIC scheme" section by providing an overview of our baseline PIC code developed at Imperial Plasma Propulsion Laboratory (IPPL). In the same section, we also review the preliminary formulation underpinning the pseudo-2D PIC scheme and summarize the computational advantages of this approach over traditional multi-dimensional PIC schemes. In "Pseudo-2D axial-azimuthal simulation" section, we discuss the axial-azimuthal pseudo-2D simulation setup and results, comparing the predictions of the pseudo-2D PIC vs a 1D axial simulation with ad-hoc Bohm mobility model against a full-2D reference simulation. In "Pseudo-2D azimuthal-radial simulation" section, we present the pseudo-2D azimuthal-radial simulation setup and discuss the predictions of the pseudo-2D simulation in this configuration compared to a 1D radial, 1D azimuthal and a full-2D PIC simulation from the literature. In "Pseudo-2D axial-radial simulation" section, we move to the axial-radial coordinates and present the pseudo-2D axial-radial simulations, comparing the observations with those from a reference 2D hybrid simulation and a series of 1D axial PIC simulations we performed with and without ad-hoc relations to account for the wall effects. Finally, we present the conclusions in "Conclusions" section in which the next steps toward further maturing the pseudo-2D PIC scheme are outlined.

IPPL particle-in-cell code and the pseudo-2D PIC scheme

Overview of the Imperial Plasma Propulsion Laboratory particle-in-cell code

The IPPL particle-in-cell code is an electrostatic, explicit kinetic simulation tool that is developed to accurately simulate the modern Hall thrusters. As a result, dedicated efforts have been spent on ensuring that the code's core modules and the subroutines capturing the physical processes such as the inter-particle collisions and plasma interactions with the channel walls are rigorously implemented. To this end, an extensive

verification campaign has been carried out by performing several module-level tests and global-level benchmarking simulations. A detailed description of the code alongside the results of its verification against the "Capacitively Coupled Discharge" benchmark [12] and in a 1D azimuthal simulation case [13] are reported in Ref. [10].

In this section, we briefly review the code's main features. Furthermore, in Plasma-wall interactions module in the IPPL PIC code of the Appendix, we introduce the wall interactions module of the IPPL code and present the code's benchmarking results in a 1D radial simulation case with conditions representative of a Hall thruster [14].

The IPPL code is written in Julia language [15] and uses the built-in Julia Random Number Generator (RNG) that follows the Xoshiro256++ algorithm [16] by default. Collisions between the plasma particles and the neutrals are resolved in this work using the Monte Carlo Collisions (MCC) scheme [17]. In this regard, the electron-neutral collision cross-sections are taken from the Biagi-v7.1 Dataset [18, 19] for all simulations we have performed in this effort.

The wall interaction module, which is used for the pseudo-2D azimuthal-radial and axial-radial simulations, incorporates multiple schemes for the Secondary Electron Emission (SEE) from the thruster's channel walls, including a simple linear model [20] and a more advanced Monte-Carlo-based model using Vaughan formulation [21].

To solve the electric potential, we have used the Thomas tridiagonal algorithm for this study. The scattering of the particle-based data onto the grid nodes and the gathering of the grid-based data onto the particles' location are carried out using a linear weighting scheme. For the sampling of macroparticles from a distribution function, the Box-Muller algorithm is used [22]. The plasma macroparticles are pushed using the classic leap-frog scheme with the magnetized electrons' push function following the Boris implementation [23].

Review of the underlying formulation and the computational advantage of the pseudo-2D PIC scheme

The pseudo-2D PIC scheme, introduced in Ref. [10], is enabled through a novel approach to approximate the 2D potential distribution in a Hall thruster as the superimposition of a series of 1D potential functions. The preliminary formulation of this decomposition of Poisson's equation was described in detail in Ref. [10] and was shown to yield a decoupled system of 1D Ordinary Differential Equations for the potential functions along the x- and y-direction of the simulation domain.

In this section, we first present a review of the formulation on which the pseudo-2D PIC scheme is based, focusing on its so-called "single-region" implementation [10]. This is, on the one hand, motivated by the fact that, as we will clarify shortly, the single-region pseudo-2D PIC simulation provides the maximum reduction in the computational cost compared to a full-2D simulation. Hence, it is of high interest to evaluate the predictions' accuracy of this very computationally efficient PIC code regarding the multi-dimensional physical processes and their couplings, an effort that will answer the first question behind this article.

On the other hand, the single-region implementation of the pseudo-2D scheme amounts to capturing an average effect of the processes along the azimuthal or radial directions in an otherwise 1D axial PIC simulation. This is, thus, consistent with the

second question that the present work aims to answer, i.e., if resolving such an average effect yields a reasonably accurate prediction of the plasma properties' axial profiles.

To present the formulation of the single-region pseudo-2D PIC scheme, we refer to Fig. 1 which shows a 2D x–y computational domain, decomposed separately into one horizontal region (Ω^x) along the x-direction (Fig. 1(a)) and one (single) vertical region (Ω^y) along the y-direction (Fig. 1(b)).

At the intersection of the axial region with the vertical one, we assume that the 2D potential field ($\phi(x,y)$) can be expressed in terms of a linear combination of two independent potential fields ϕ^x and ϕ^y, where ϕ^x and ϕ^y are, respectively, the potential fields in region Ω^x and in region Ω^y. Thus, we write

$$\phi(x,y) = C^x\phi^x + C^y\phi^y, \text{with } x \in \Omega^x, y \in \Omega^y. \tag{1}$$

In the above equation, C^x and C^y are the weighting coefficients used to approximate the 2D potential field, with C^x being constant in Ω^x and, likewise, C^y being constant in Ω^y. The potential functions ϕ^x and ϕ^y are, by definition, only a function of the x- and the y-direction, respectively, and can, hence, be obtained from 1D Poisson's equations.

We now perform a change of variables in Eq. 1 and define

$$\zeta(x) = C^x\phi^x(x), \tag{2}$$

$$\eta(y) = C^y\phi^y(y), \tag{3}$$

such that, $\phi(x,y) = \zeta(x) + \eta(y)$ at the regions' intersection. Accordingly, the 1D Poisson's equations for the potential functions ϕ^x and ϕ^y can be written as follows in terms of the functions $\zeta(x)$ and $\eta(y)$

$$\frac{d^2\zeta(x)}{dx^2} = -C^x\frac{\rho^x(x)}{\epsilon_0}, \tag{4}$$

$$\frac{d^2\eta(y)}{dy^2} = -C^y\frac{\rho^y(y)}{\epsilon_0}, \tag{5}$$

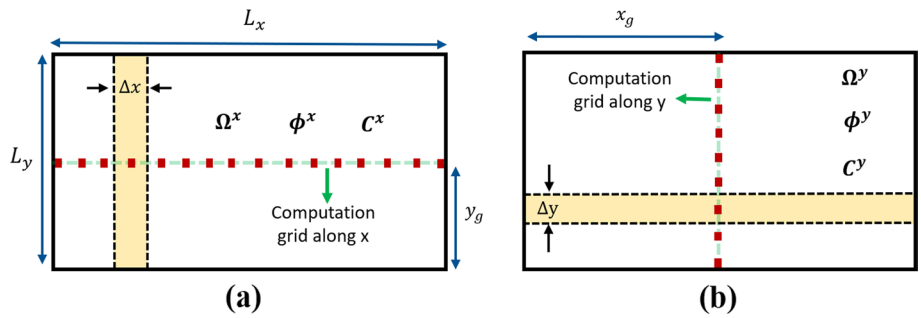

Fig. 1 Schematics of the computational domain and the defined "Regions"; (**a**) the horizontal region (Ω^x), and (**b**) the vertical region (Ω^y). x_g and y_g are, respectively, the locations from the origin of the computation grid along y and x

for computational cells extending over the entire width of the regions, i.e., the highlighted areas in Fig. 1(a) and (b). In Eqs. 4 and 5, ϵ_0 is the permittivity of free space. Additionally, ρ^x and ρ^y are, respectively, the average of the 2D charge density distribution $\rho(x,y)$ over the y-direction and the x-direction of the domain, calculated as

$$\rho^x(x) = \frac{1}{L_y}\int_0^{L_y} \rho(x,y)dy, \tag{6}$$

$$\rho^y(y) = \frac{1}{L_x}\int_0^{L_x} \rho(x,y)dx. \tag{7}$$

Concerning the weighting coefficients C^x and C^y, we assumed their values to be the same and equal to 0.5 for all simulations presented in this study. In this respect, in Ref. [10], we performed detailed analyses on the sensitivity of the code's results to the value of these coefficients for the axial-azimuthal pseudo-2D simulations using the single-region implementation. We found that the scheme's predictions and stability remain almost invariant as far as $C^y \geq C^x$. A similar conclusion has been drawn in the azimuthal-radial and axial-radial configurations through performing a preliminary analysis on the sensitivity of the results to these coefficients. We noticed that an equal selection of the weighting coefficients is always a reliable choice.

Finally, from the numerical implementation perspective, the decoupled Eqs. 4 and 5 have been solved separately using the Thomas Tridiagonal algorithm in all pseudo-2D simulation cases. The electric field was in turn calculated using the relation $\overrightarrow{E} = -\overrightarrow{\nabla}\phi(x,y) = -\overrightarrow{\nabla}\left(\zeta(x) + \eta(y)\right)$.

Having reviewed the preliminary underlying formulation of the single-region pseudo-2D PIC, we briefly present the computational benefit of the approach. In this respect, we emphasize that, as illustrated in Fig. 1, the single-region implementation amounts to decomposing the 2D PIC problem into two in-parallel 1D problems along the x and y directions of the simulation domain. This implies that the number of computational cells is reduced from $O(N^2)$ corresponding to a full-2D simulation to $O(N)$, which is effectively equivalent of a 1D PIC simulation. In turn, considering that the same initial number of macroparticles per cell as in a 2D simulation case is used for a single-region pseudo-2D simulation, the *total* initial number of macroparticles would be two orders of magnitude lower in the single-region simulation compared to a full-2D simulation. This reduction in the number of cells and the total number of macroparticles is translated directly into significantly lower necessary computational resources. For instance, our pseudo-2D axial-azimuthal simulation took 3 days to complete using only a single CPU core on a standard personal workstation, whereas the participating 2D codes in the benchmarking activity [24] required about 2.5 to 11 days for a complete run when using about 100 to 360 CPU cores.

Pseudo-2D axial-azimuthal simulation

As it was pointed out in "Introduction" section, azimuthal instabilities are demonstrated to have a significant role in enhancing the electrons' cross-field mobility in Hall thrusters [2]. As a result, in a kinetic PIC simulation, self-consistency with respect to electron transport can only be achieved when the azimuthal coordinate is resolved. A PIC

simulation that does not include the azimuthal coordinate requires a model to incorporate the effect of the instability-induced mobility into the simulation as an additional ad-hoc collision process.

In this section, we present the results of three simulations we have performed, comparing the results against the full-2D axial-azimuthal benchmark of Ref. [24]. The simulations that we report here include a single-region pseudo-2D axial-azimuthal simulation, a 1D axial simulation with an ad-hoc Bohm-type collision frequency profile, and a 1D axial simulation with no ad-hoc collisionality.

Simulation setup

The setup of the pseudo-2D axial-azimuthal simulation is similar to that reported in Ref. [24] and explained in detail in our previous publication [10]. Here, we provide an overview of the setup. The 1D axial simulations follow the same setup and initial conditions, with the only difference being that Poisson's equation is not solved along the y-coordinate in these 1D simulations.

The pseudo-2D simulation domain is a Cartesian $(x-y)$ plane with x along the axial direction and y along the azimuth. The domain length, cell size, timestep, total simulation time and the initial plasma and boundary conditions are those reported in Table 1 of Ref. [24].

A cosine-shaped ionization source and a bi-Gaussian magnetic field profile identical to those used in Ref. [24] were imposed. The magnetic field peak intensity is set to 100 Gauss and a maximum ion current density (J_{iM}) of 400 A/m^2 is assumed to determine the peak value of the ionization source.

The implementation of particles and potential boundary conditions are also as described in Ref. [24]. A current-equality condition is used for electrons' reinjection, which are introduced into the simulation at an injection plane on the cathode side 1 mm before the end of the domain.

The simulations were started with an initial number of macroparticles per cell of 150 along the x-direction. This corresponds to a total initial macroparticle count of 75,000 which, for the pseudo-2D simulation, translates into about 300 macroparticles per cell along the azimuthal (y) direction. In "Sensitivity of the single-region axial-azimuthal simulation to the initial number of macroparticles per cell" section of the Appendix, we have presented the single-region pseudo-2D axial-azimuthal simulation results for various initial numbers of macroparticles per cell along the azimuthal coordinate and have discussed the sensitivity of the pseudo-2D results to this parameter.

Before proceeding to the next section, we also describe the approach pursued to obtain the profile of the Bohm collision frequency that was used in the corresponding 1D axial PIC simulation as the ad-hoc electron transport model. To this end, we took the plasma potential profile of the 2D benchmark simulation, reported in Ref. [25], as the reference to tune the ad-hoc transport model. We adopted a three-zone Bohm-type transport model of the general form $\nu_{Bohm} = \left(\frac{1}{\beta}\right)\omega_c$. In this relation, $\beta = \frac{\omega_c}{\nu_e}$ is the Hall parameter with ν_e being the effective electron collision frequency, ω_c is the electron cyclotron frequency, and ν_{Bohm} is the Bohm collision frequency. This ad-hoc model was included in the PIC simulation as a fictitious isotropic-scattering collision mechanism.

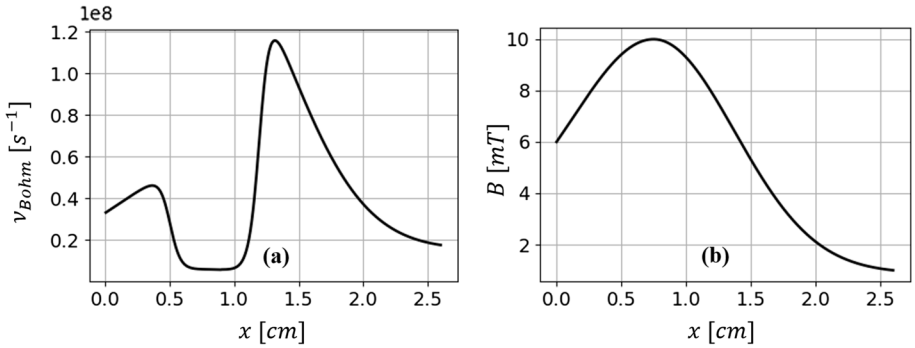

Fig. 2 (**a**) Axial profile of the Bohm collision frequency tuned on the plasma potential profile from the 2D benchmark simulation [25]; (**b**) axial distribution of the radial magnetic field for the pseudo-2D axial-azimuthal and the 1D axial simulations

It is worth pointing out that adopting a three-zone transport model was inspired by our previous works [26, 27] in which we showed that the axial profile of the instability-induced electron transport in Hall thrusters can be determined by considering a dominant physical mechanism for each of the three zones of the ionization, acceleration, and near-plume in a Hall thruster domain.

Figure 2 shows the tuned profile of the Bohm collision frequency alongside the axial distribution of the radial magnetic field. In Fig. 2(a), the transition from one zone to another is smoothed out using a Sigmoid function. The tuned collision frequency profile was used in the 1D axial PIC simulation whose results are shown in the next section. The values of β corresponding to the Bohm collision frequency profile in Fig. 2(a) are: 32 for the "ionization" zone ($0 < x \leq 0.5cm$), 300 for the "acceleration" zone ($0.5 < x \leq 1.2cm$) and 10 for the "near-plume" zone ($1.2cm < x \leq 2.5cm$).

An interesting observation to point out is that the axial distribution of the tuned "anomalous" collision frequency in Fig. 2(a) is consistent with the results of our previous works [26, 27] in which we had obtained a similar profile, but by attributing the enhanced electron mobility in each of the three zones to a specific dominant instability.

Results and discussion

Figure 3 presents the time variation of the electron current density as a ratio of the total ion current density ($J_{iM} = 400A/m^2$) from the single-region pseudo-2D axial-azimuthal simulation. The electron current is calculated in the same manner as that reported in Ref. [24]. It is observed that, after an initial transient, the simulation has arrived at steady state at about 10 μs from which point, the normalized electron current density J_e/J_{iM} shows a low-amplitude, low-frequency oscillation around the mean value of about 75%. The same temporal behavior of the normalized electron current density is reported in Ref. [24]. Furthermore, the mean value of the ratio J_e/J_{iM} from our single-region simulation at steady state is confirmed to be the same as that from the 2D benchmark simulations [24].

Figure 4 shows the comparison in terms of the axial profiles of the time-averaged plasma properties between the 2D axial-azimuthal benchmark and our three simulations, i.e., the single-region pseudo-2D, 1D axial with ad-hoc Bohm collisionality, and 1D axial without any ad-hoc collisionality.

First, in Fig. 4(c), where the plasma potential profile from the 1D axial simulation without any ad-hoc collisionality is shown, it is observed that, in the absence of any mechanism, either artificially introduced or self-consistently resolved, to take into account the enhanced cross-field transport in the simulation, the axial mobility of electrons is insufficient and, thus, the plasma potential cannot be sustained.

Second, it is seen in Fig. 4 that incorporating the tuned Bohm collision frequency profile (Fig. 2(a)) in the 1D axial simulation yields quite similar results with respect to the full-2D simulation. This implies that the three-zone approach to represent the "anomalous" cross-field mobility [26, 27] can be a viable method for the plasma simulations of Hall thrusters. However, while rigorous closure models do not exist to link the cross-field mobility to the variations in the plasma properties based on the underlying physical processes, the need to tune the ad-hoc transport profile for each specific simulation condition remains as the main disadvantage of the approaches that rely on externally introducing anomalous mobility in the simulation.

Finally, the self-consistent predictions of the pseudo-2D simulation are observed to be consistent with the 2D profiles. It is underlined that the single-region simulation is capturing an axially averaged effect of the azimuthal instabilities on the axial transport of electrons, which is nonetheless seen to result in a reasonably accurate estimate of the distribution of the plasma properties that is feasible with an average representation of the azimuthal physics. Furthermore, the single-region simulation results are also similar to those from the 1D axial simulation with Bohm mobility, implying that the pseudo-2D scheme, even in its simplest single-region implementation, can obviate the need for ad-hoc transport models in PIC codes.

We now look more closely into the capability of the single-region pseudo-2D PIC simulation in resolving the underlying physics.

In this regard, we first examine the phase-space diagrams of the ions in the $x-u$ and $y-v$ planes, with x representing the axial coordinate, y representing the azimuthal coordinate, and u and v being, respectively, the axial and azimuthal velocity components of the ions. The phase-space plots are shown in Fig. 5 and correspond to the distribution of the ions in the 1D1V phase spaces at the steady state. Figure 5(a) presents the phase-space diagram of the ion axial velocities, which is consistent with

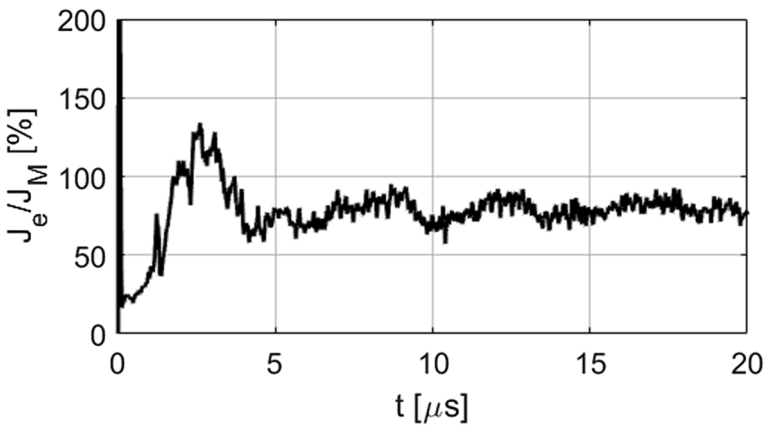

Fig. 3 Temporal evolution of the electron current density (J_e) as a ratio of the total ion current density (J_M) from the single-region pseudo-2D axial-azimuthal simulation

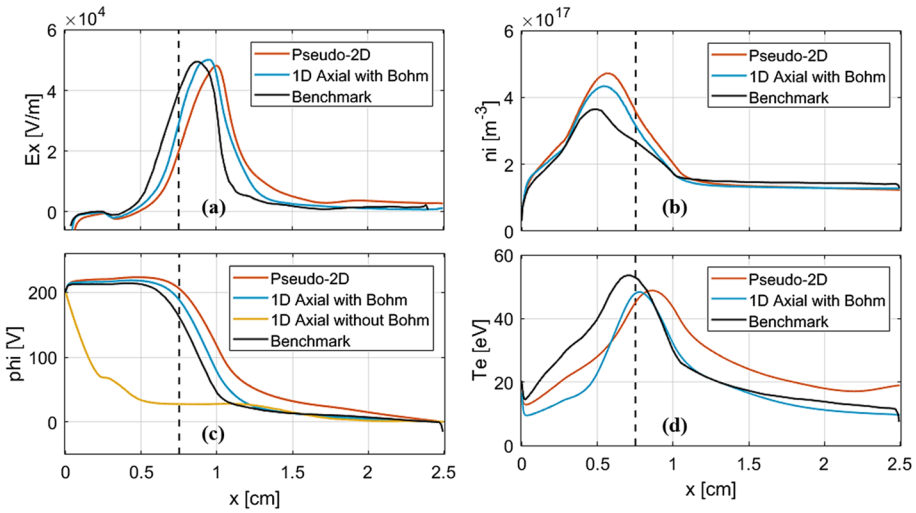

Fig. 4 Comparison between the axial distribution of the time-averaged plasma properties from the single-region pseudo-2D simulation, a 1D axial simulation with ad-hoc Bohm mobility, and the 2D benchmark case [24]; (**a**) electric field, (**b**) ion number density, (**c**) plasma potential, and (**d**) electron temperature. In plot (**c**), the plasma potential profile from the 1D axial simulation without any ad-hoc collisionality is shown as well

the similar plots reported in the literature, for instance, from the 2D simulations carried out in Ref. [28]. It is observed that the majority of the ions are accelerated to exhaust velocity values close to the theoretical value of about 18 km/s for a potential drop of 220 V (Fig. 4(c)). However, a velocity spread is also observed, indicating the presence of a relatively slow ion population.

Along the azimuthal direction (Fig. 5(b)), the phase-space diagram of the ion azimuthal velocities clearly shows the trapping of the ions due to interaction with the azimuthal waves. This demonstrates that the pseudo-2D simulation has captured the important ion-wave trapping phenomenon, which is reported in the literature [28] as the saturation mechanism for the azimuthal instability resolved by our pseudo-2D simulation.

To elaborate on the nature and characteristics of the resolved azimuthal waves, we refer to Fig. 6. In this regard, Fig. 6(a) illustrates the spatiotemporal map of the azimuthal electric field, and Fig. 6(b) shows the dispersion map of the azimuthal electric field fluctuations in the $(k_y - \omega)$ plane, where k_y is the azimuthal wave number and ω is the real frequency component. The x- and y-axis in the dispersion plot in Fig. 6(b) are normalized, respectively, with respect to the Debye length (λ_D) and the local ion plasma frequency (ω_{pi}). Moreover, the theoretical dispersion relation of ion acoustic waves in the ions' reference frame (Eq. 8) [29] is superimposed on the dispersion map in Fig. 6(b). In Eq. 8, C_s is the ion sound speed.

$$\omega \approx \frac{k_y C_s}{\sqrt{1 + k_y^2 \lambda_D^2}}. \tag{8}$$

It is observed that the dispersion map of the resolved azimuthal instabilities shows a very good agreement with the theoretical dispersion relation, an aspect which is in

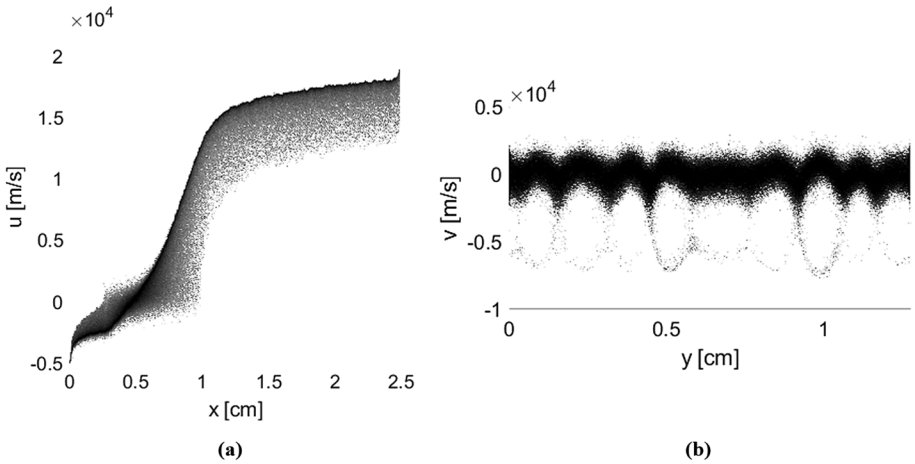

Fig. 5 1D1V phase-space diagrams of the ions from the single-region pseudo-2D simulation; (**a**) distribution of ion axial velocities (u) along the axial direction, (**b**) distribution of ion azimuthal velocities (v) along the azimuthal direction

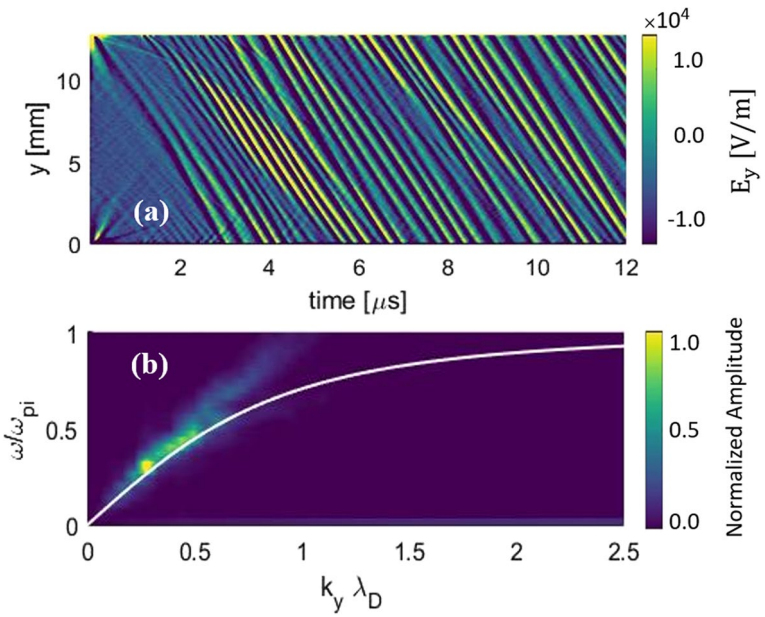

Fig. 6 Time evolution of the azimuthal electric field (**a**), and the corresponding dispersion map (**b**) from the single-region pseudo-2D axial-azimuthal simulation. Amplitudes in (**b**) are normalized with that of the most dominant mode

line with the observations from 2D PIC simulations [24]. Furthermore, the characteristics of the azimuthal waves in terms of the real frequency ($\omega \sim 3MHz$) and wavelength ($\lambda \sim 2mm$) are consistent with the literature on the modified ion acoustic instability in Hall thrusters [25].

Accordingly, it is possible to conclude that the single-region simulation provides an accurate average representation of the azimuthal waves in Hall thrusters.

Pseudo-2D azimuthal-radial simulation

In line with the objectives defined for this work in "Introduction" section, we carried out a single-region azimuthal-radial simulation to verify the extent to which the pseudo-2D PIC scheme with its preliminary formulation can capture the interplay between the radial and azimuthal plasma processes in comparison with a full-2D azimuthal-radial reference simulation [20]. To this end, we also performed a 1D radial and a 1D azimuthal simulation and assessed the capability of the pseudo-2D scheme to resolve two main interactions reported in the literature between the azimuthal instabilities and the near-wall sheath; namely, the heating of the plasma electrons by the instabilities and the consequent variation in the SEE regime that can influence the electrons' axial mobility [5], and the role of the secondary emitted electrons from the walls in moderating the azimuthal waves' energy [20].

Before proceeding further, we acknowledge the recent development of an azimuthal-radial benchmark case in the community [30]. However, we found the results from the benchmarking activity of Ref. [30] incompatible with the objectives we had defined for our pseudo-2D studies here in the azimuthal-radial configuration. Accordingly, as pointed out in the preceding paragraph, we adopted as reference the simulation case described in Ref. [20].

Simulation setup

The setup of the single-region pseudo-2D simulations in the azimuthal-radial configuration is similar to the one used in Ref. [20] for full-2D simulations in this same configuration. The 1D radial and 1D azimuthal simulations, whose results are presented in the next section for comparison with the pseudo-2D results, have the same setup and conditions as the pseudo-2D case but being adapted accordingly for 1D simulations.

The simulation domain is essentially a 2D $(x-y)$ Cartesian plane with the x-coordinate along the azimuthal direction and the y-coordinate along the radius. The domain azimuthal (L_x) and radial $\left(L_y\right)$ extents are 0.5 cm and 2 cm, respectively. A constant and uniform axial electric field of $2 \times 10^4 \frac{V}{m}$ and a radial magnetic field of 200 G are imposed. Initially, electrons and ions are sampled from a Maxwellian distribution at the temperatures of 5 eV and 0.1 eV, respectively, and are loaded uniformly throughout the domain with the density of $3 \times 10^{17}\mathrm{m}^{-3}$. A background of immobile neutrals with a uniform density of $3.22 \times 10^{19}\mathrm{m}^{-3}$ is assumed for the electron-neutral collisions, which consist of a single ionization, four excitations, and the elastic momentum-transfer collision.

A finite axial length $(L_x = 1cm)$ is assumed for the domain in the 1D azimuthal and pseudo-2D azimuthal-radial simulations. Particles crossing the domain boundaries in the axial direction are resampled from their initial distribution function and reinjected from the opposite boundary. During reinjection in the pseudo-2D simulation, a particle keeps the radial position at which it has crossed the boundary but is loaded at a random azimuthal location. As suggested in Ref. [13], introducing a finite axial length in the simulation and removing the particles that cross this axial boundary allows us to mimic the convection of the azimuthal instabilities, which is important to properly capture the saturation of the waves' energy.

Concerning the wall boundaries along the radial direction, a grounded wall is assumed. For the simulations where the Secondary Electron Emission is resolved, a linear model for the SEE yield (Eq. 9) [20] is considered.

$$\gamma = \max(\gamma_{max}, \gamma(\omega)); \gamma(\omega) = \gamma_0 + \frac{\omega}{\omega^*}(1 - \gamma_0). \tag{9}$$

In Eq. 9, γ_{max} is the maximum electron emission coefficient, γ_0 is the probability of attachment, and ω^* is the crossover energy. For our simulations below, we have used the values of the above parameters for Boron Nitride, i.e., $\gamma_{max} = 2.9$, $\gamma_0 = 0.578$ and $\omega^* = 35.04$eV. The secondary electrons are emitted at the assumed temperature of 1 eV.

As the simulation does not account for the axial inflow and outflow of the particles self-consistently, the particles' flux toward the wall needs to be compensated artificially. To this end, we followed the approach described in Ref. [20]. The radial fluxes are compensated by injecting electron–ion pairs randomly in the domain at each timestep. In order not to disturb the non-neutrality in the sheath, the number of pairs to inject is estimated as the minimum between the number of electrons and the number of ions reaching the wall at every timestep.

Table 1 provides a summary of the numerical parameters and plasma conditions used for the pseudo-2D azimuthal-radial simulations.

Results and discussion

Coupling of the sheath processes to the azimuthal instabilities and changes in the SEE regime

In Fig. 7, we compare the temporal evolution of the sheath from the single-region pseudo-2D simulation with that from the 1D radial simulation. Looking at the plots on the left- and right-hand side columns of Fig. 7, it is clear that the sheath dynamics is completely different. First, the plasma potential in Fig. 7(a) shows a large-scale periodic

Table 1 Summary of the numerical and physical parameters used for the pseudo-2D azimuthal-radial simulations

Parameter	Value [unit]
Computational Parameters	
Time step (Δt)	4×10^{-12}[s]
Total simulation time (t_{final})	12×10^{-6}[s]
Azimuthal domain length (L_x)	0.5 [cm]
Radial domain length (L_y)	2.0 [cm]
Axial domain length (L_z)	1.0 [cm]
Cell size ($\Delta x = \Delta y$)	2×10^{-3}[cm]
Initial number of macroparticles per cell for azimuthal grid (N_{ppc_x})	200
Initial number of macroparticles per cell for radial grid (N_{ppc_y})	50
Physical Parameters	
Plasma density (n_p)	3×10^{17}[m^{-3}]
Neutral gas density (n_n)	3.22×10^{19}[m^{-3}]
Electron injection temperature (T_e)	5.0 [eV]
Ion injection temperature (T_i)	0.1 [eV]
Axial electric field ($E_{x,0}$)	2×10^4[V/m]
Radial magnetic field ($B_{r,0}$)	200 [Gauss]

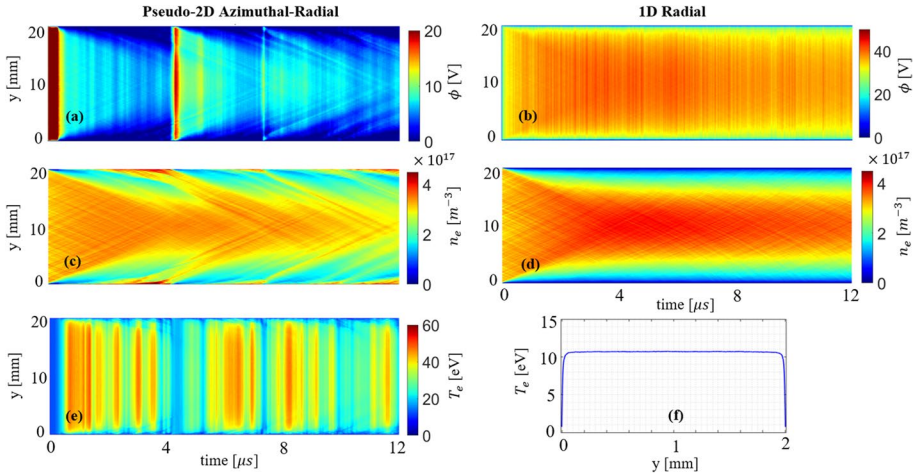

Fig. 7 Comparison between the sheath characteristics from the pseudo-2D azimuthal-radial vs the 1D radial simulation; (**a**) & (**b**) plasma potential (ϕ), (**c**) & (**d**) electron number density (n_e), and (**e**) & (**f**) electron temperature (T_e)

behavior, whereas Fig. 7(b) shows a rather stable sheath throughout the simulation time. Second, streams of secondary electrons emitted from the walls propagate toward the bulk plasma in the center of the domain (Fig. 7(c)) while no such behavior is observed in the 1D radial case (Fig. 7(d)). This is an indication of a strong SEE in the presence of the azimuthal waves. Finally, whereas the electron temperature evolution in the pseudo-2D case features periodic rise and drop (Fig. 7(e)), the electron temperature in the radial case (Fig. 7(f)) was almost constant in time and, thus, the time-averaged distribution is displayed.

The intriguing features seen in Fig. 7 are now explained: it is important to recall, first, that the excitation and growth of the azimuthal instabilities in the pseudo-2D simulation results in the thermalization of the electron population. This, in turn, increases the sheath potential drop and translates into a higher SEE rate. These effects can be better understood by referring to the plots in Fig. 8. In Fig. 8(a), the increase in the kinetic energy of electrons and ions is the evidence of the energy transfer from the azimuthal waves to the particles. As these waves are absent in the 1D radial simulation (Fig. 8(b)), the electrons' energy remains almost constant while the ions' energy decreases due to the injection of low-energy Maxwellian ions into the system used to maintain the plasma in our simulations involving the radial coordinate.

As the energy of the electrons increases, so does too the SEE yield coefficient, which exceeds the threshold corresponding to the Space-Charge-Saturated (SCS) regime at about 1 μs into the simulation (Fig. 8(c)). At around 4 μs, a "burst" event occurs where a high-density stream of near-wall electrons travel toward the bulk plasma (Fig. 7(c)). This event is associated with a drop in the SEE yield to below the SCS limit, marked by a horizontal red dashed line in Fig. 8(c). The propagation of this beam toward the center of the domain disrupts the azimuthal waves and lowers the electrons' kinetic energy and temperature. The secondary electron beam reaches the center at about 7 μs, quenching the electron temperature in the bulk (Fig. 7(e)). This is followed by another small

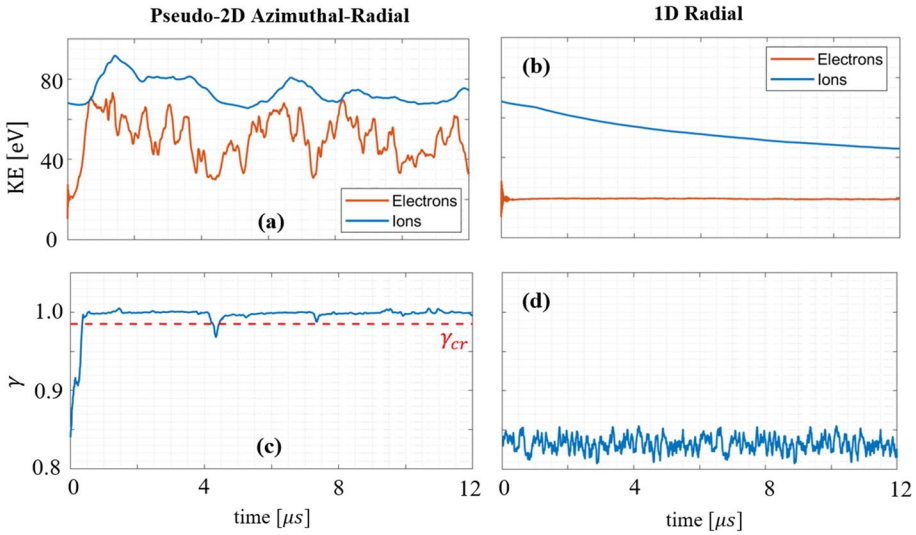

Fig. 8 Time evolution of the kinetic energy and SEE yield coefficient from the pseudo-2D radial-azimuthal (left column) and 1D radial (right column) simulations; (**a**) and (**b**) electrons' and ions' kinetic energy, (**c**) and (**d**) SEE yield coefficient (average of the two walls)

"burst" event (Fig. 7(c)), together with a minor drop in the SEE yield (Fig. 8(c)). After these events, the sheath seems to be stabilizing in the SCS regime with a SEE yield coefficient of about 1.

This dynamic behavior and stabilization of the SEE yield have been also observed in the reference 2D azimuthal-radial simulation [20]. In particular, Ref. [20] has identified various regimes for the sheath behavior in the presence of SEE, which depend on the value of the cross-over energy of the channel wall material. For cross-over energy values (ω^*) below 40 eV, it is specified in Ref. [20] that the SCS regime becomes stable after a few initial "burst" events, and the SEE yield coefficient stabilizes at a value close to and slightly below 1.

As in our pseudo-2D simulation, we had adopted a crossover energy value of 35.04 eV, it was intended to verify if we could recover a similar regime of sheath behavior as that reported in Ref. [20] for ω^* values below 40 eV. In this respect, the consistency between the psuedo-2D and full-2D simulations' prediction of the sheath regime demonstrate that the single-region PIC can rather reasonably capture the impact of the azimuthal instabilities on the sheath behavior and the Secondary Electron Emission phenomenon.

Effects of the radial physics on the azimuthal instabilities' characteristics and the instability-induced electron transport

In this section, we discuss the observations from our pseudo-2D azimuthal-radial simulation related to the effects of radial gradients and plasma-wall interactions on the behavior of the azimuthal instabilities and, in particular, their induced electron transport.

In this regard, we compare in Fig. 9 the evolution of the average electrons' axial mobility and the particles' energy obtained from the pseudo-2D simulations against those from 1D azimuthal simulations in the presence and in the absence of SEE. In these plots, μ_{eff} is the enhanced mobility, which is the sum of the instability-induced and

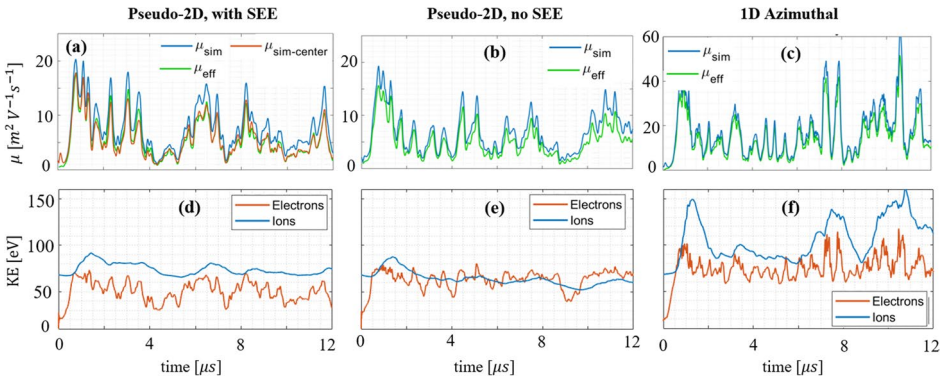

Fig. 9 Top row: time evolution of average electrons' axial mobility, Bottom row: time evolution of particles' average kinetic energy. (**a**) & (**d**) are from single-region pseudo-2D simulation with linear SEE model; (**b**) & (**e**) from pseudo-2D simulation with no SEE; and (**c**) & (**f**) are from the 1D azimuthal simulation

classical mobility as given by the theoretical relation in Eq. 10 [13]. In addition, μ_{sim} and $\mu_{sim-center}$ are the average electrons' mobility obtained from the simulations using Eq. 11. The difference between these terms is that, for μ_{sim}, the average is taken over the particles in the entire radial extent, whereas for $\mu_{sim-center}$ only the particles whose radial positions are within the range of $0.25L_y$ and $0.75L_y$ are considered. The reason behind this distinction in the calculation of the mobility terms from the simulations is to distinguish the role of Near-Wall Conductivity process, which is absent in $\mu_{sim-center}$.

$$\mu_{eff} = \frac{\frac{e}{m_e \nu_c}}{1 + \left(\frac{\omega_c}{\nu_c}\right)^2} \left(1 - \frac{\omega_c}{\nu_c} \frac{\langle \widetilde{n}_e \widetilde{E}_x \rangle}{n_e E_z}\right), \tag{10}$$

$$\mu_{sim} = \left| \frac{\sum_{i=1}^{N} v_{z_e}}{N E_z} \right|. \tag{11}$$

In Eq. 10, ν_c is the electron-neutral momentum transfer collision frequency, n_e is the time-averaged electron number density and E_z is the axial electric field. Moreover, the term $\langle \widetilde{n}_e \widetilde{E}_x \rangle$ represents the average of the product of azimuthal fluctuations in the electron number density ($\widetilde{n}_e$) and the azimuthal electric field ($\widetilde{E}_x$) over the entire azimuthal domain and over a time interval (Δt) that is larger than the characteristic time of the instabilities [13]

$$\langle \widetilde{n}_e \widetilde{E}_x \rangle = \frac{1}{\Delta t} \frac{1}{L_x} \int_0^{\Delta t} \int_0^{L_x} \widetilde{n}_e(x,t) \widetilde{E}_x(x,t) dx dt. \tag{12}$$

In Eq. 11, v_{z_e} is the axial electrons' drift velocity and N is the number of macroparticles.

Now, looking at the plots in Fig. 9, it is, first, observed that, in all cases, μ_{sim} is in great agreement with μ_{eff}. Second, the particles' energy and the electrons' mobility are higher in the 1D azimuthal simulation with respect to the pseudo-2D simulations. This is in line with Fig. 10(f), which shows that the waves' potential energy (and, hence, the waves' amplitude) is larger in the 1D azimuthal case. Therefore, including the radial direction

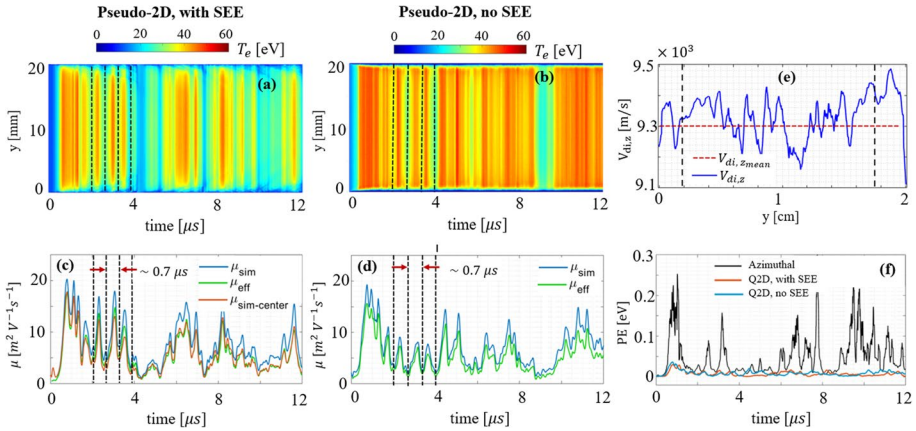

Fig. 10 Time evolution of the radial distribution of the electron temperature in (**a**) pseudo-2D simulation with linear SEE model and (**b**) pseudo-2D simulation with no SEE. Time evolution of the average electrons' mobility is shown in (**c**) for the pseudo-2D simulation with linear SEE model and in (**d**) for the pseudo-2D simulation with no SEE. Plot (**e**) is the radial distribution of ions' axial velocity averaged over the last 2 μs of simulation's time. The dashed red line is the mean axial velocity over the radius. Plot (**f**) is the comparison between the azimuthal waves' potential energy in the pseudo-2D simulation with and without SEE and in the 1D azimuthal simulation

has clearly limited the growth of the instability, which is consistent with the reference full-2D simulation results [20].

Third, the difference between μ_{sim} and $\mu_{sim-center}$ in Fig. 9(a) indicates the existence of Near-Wall Conductivity phenomenon at the Space-Charge-Saturated limit of the sheath. The 2D simulation results of Ref. [20] have also shown a similar trend. Moreover, the electrons' energy in the presence of SEE, shown in Fig. 9(d), is lower with respect to the "no-SEE" simulation because the emission of low-temperature secondary electrons from the walls reduces the average energy of the electrons' population. This point is evident as well in the electrons' temperature maps shown in Fig. 10(a) and (b).

Finally, it is important to highlight that the large-amplitude oscillations observed in the electrons' mobility (Fig. 10(c) and (d)), which are correlated with the oscillations in the electrons' temperature (Fig. 10(a) and (b)) are not physical. These oscillations are the artifact of the assumed finite axial extent and the reinjection of particles into the domain, which have been also noticed in the full-2D azimuthal-radial simulations of Ref. [20].

To support the above statement, we refer to Fig. 10(e), which shows the radial distribution of the ions' average axial velocity. According to this plot, the characteristic axial transit time of the ions across the artificial axial length of 1 cm can be calculated to be about $1.1\mu s$, which is comparable with the period of the oscillations in electrons' temperature and mobility ($\sim 0.7\mu s$). Therefore, when the majority of ions reach the right-hand-side end of the domain and get reinjected from the left-hand-side, a new cycle begins, and this constant particle reinjection prevents the establishment of a proper steady-state condition for the waves.

The above results, discussed in "Coupling of the sheath processes to the azimuthal instabilities and the changes in the SEE regime" section and "Effects of the radial

physics on the azimuthal instabilities' characteristics and the instability-induced electron transport" section, confirm that the pseudo-2D scheme has the potential to resolve the mutual interactions between the azimuthal and radial physical processes, predicting consistently the same interplay between these phenomena as that observed in 2D PIC simulations in the azimuthal-radial coordinates.

Pseudo-2D axial-radial simulation

The interactions of the plasma with the channel walls can have two main effects on the axial distribution of the plasma properties: on the one hand, the electrons reaching the wall or getting reflected by the sheath lose part of their kinetic energy. This limits the rate of ionization that is directly proportional to the electrons' energy. Furthermore, secondary emitted electrons from the walls lower the overall temperature of the electrons' population and, thus, play an additional role in regulating the ionization. Changes in the electrons' energy and, consequently, the ionization rate affects the plasma density profile and the extent of the ionization zone.

On the other hand, electron-wall collisions and the Near-Wall Conductivity phenomenon can play a non-negligible role in the electrons' axial mobility [2]. The higher the wall-induced electron transport, the lower would be the self-consistent electric field, which affects both the ionization and the acceleration processes.

As a result, it is important to have a reliable approach to resolve the effects of the wall interactions in a predictive kinetic simulation. Accordingly, in this section, we present the results of our pseudo-2D axial-radial simulations and compare the results against 1D axial PIC simulations with and without a model to account for the plasma-wall interactions. To have a point of reference, the setup of all simulations is similar to a recent 2D hybrid fluid/PIC simulation from the literature [31], and our results are compared against those from the hybrid code. In this regard, it is important to highlight that an axial or axial-radial PIC simulation is not self-consistent with respect to electron mobility and, as a result, the same model as that in Ref. [31] to account for the enhanced electrons' cross-field transport is included in our 1D and pseudo-2D simulations in this section. As such, since the choice of electrons' mobility model can have a dominant influence on the plasma dynamics, it was expected that the results would be mostly comparable, which will be seen in "Results and discussion" section to has been the case.

It is also important to recall that, as mentioned in "Introduction" section, by performing the single-region pseudo-2D axial-radial simulations, we aim to demonstrate preliminarily that this approach can provide a self-consistent method to capture an average effect of the plasma-wall collisions and the associated particles' momentum and energy loss in lieu of the ad-hoc models that have been proposed in the literature for this purpose [3, 31].

Simulation setup

The domain of the simulations is a rectangular Cartesian plane, resembling the channel and the immediate near-plume zone downstream the exit plane of the SPT-100 Hall thruster. The x-axis is along the channel axis and the y-axis is along the radial direction. The axial extent of the domain was chosen to be 3 cm compared to 6 cm in Ref. [31]

in order to speed up the simulation by reducing the number of macroparticles. In the y-direction, however, the same extent of 1.5 cm as in Ref. [31] was used. The simulated operating condition is the same as that adopted in Ref. [31], with the discharge voltage being 300 V and the anode mass flow rate being 5 mg/s. The axial profile of the radial magnetic field is the one shown in Fig. 9 of Ref. [31] with the peak intensity of 16 mT.

At the beginning of the simulation, the electrons and ions are sampled from a Maxwellian distribution at 10 eV for the electrons and 0.5 eV for the ions. These particles are then injected uniformly throughout the domain at exactly same locations. In order to maintain the discharge, electrons are sampled from a half-Maxwellian at 10 eV and are injected into the domain from the cathode boundary at each timestep. The number of electrons to inject is determined based on the quasineutrality approach [25].

An anode temperature of 750 K and a wall temperature of 850 K were assumed, consistent with the corresponding values in Ref. [31]. The neutral particles are sampled from a Maxwellian at the anode temperature and are loaded into the domain according to an initial profile given in Ref. [8]. The neutral density at the anode at the beginning of the simulation is $3.22 \times 10^{19} \mathrm{m}^{-3}$. The evolution of the neutrals' population is traced kinetically.

In all simulations, the neutrals created due to ion recombination on the anode are sampled from a half-Maxwellian at the anode temperature. Moreover, for the pseudo-2D simulation, the ion recombination on the channel walls is also considered and the corresponding neutrals are sampled from a half-Maxwellian at the wall temperature.

Concerning the plasma-wall interactions, the SEE phenomenon is resolved self-consistently in the pseudo-2D simulation using the Monte-Carlo-based Vaughan model [21]. The secondary electrons are sampled from a half-Maxwellian at the assumed temperature of 2 eV and are diffusely injected into the domain. For the 1D axial simulation with an ad-hoc wall-collision model, the following approach, originally introduced in Ref. [32], was used: a collision frequency (ν_{wall}) was included in an empirical manner as.

$$\nu_{wall} = \alpha_w \nu_{w,exp} \tag{13}$$

in which, α_w is a free parameter (here assumed to be 0.1), and $\nu_{w,exp}$ is an experimentally measured electron-wall collision frequency (typically $10^7 s^{-1}$). This determines the frequency with which the electrons lose momentum in colliding with the wall. Another relation is invoked to model the energy loss corresponding to either a wall collision or other "anomalous" mechanisms, expressed as [32]

$$\mathcal{W} = \epsilon \exp\left(-\frac{\mathcal{U}}{\epsilon}\right), \tag{14}$$

where ϵ is the electron kinetic energy in eV, and $\mathcal{U}$ is a threshold electron energy (empirically set at 20 eV). In the PIC simulation, the above electron-wall collision model was included as a fictitious collision event within the MCC module with the frequency and the energy loss given by Eqs. 13 and 14.

The electrons were also assumed to collide with neutrals and the following collision events were resolved through the MCC scheme: the single ionization, four excitations and the elastic momentum-transfer collision.

Concerning the enhanced electrons' axial mobility, noting that the simulations reported here do not resolve the azimuthal coordinate, an ad-hoc electron mobility model based on the Bohm collision frequency, similar to that described in "Simulation setup" section for the axial-azimuthal simulations, was implemented. In this regard, to be consistent with the reference 2D hybrid simulation [31], we used a "two-zone" model of the general form $\nu_{Bohm} = (\frac{\alpha}{16})\omega_c$, with the tuning coefficient α being 0.035 inside the channel and 5 in the near-plume.

Table 2 presents a summary of the numerical parameters and plasma conditions used for the pseudo-2D axial-radial simulations. The same parameters and conditions, where applicable, are also used for the 1D simulations.

Results and discussion

Figure 11 shows the axial distribution of the time-averaged plasma properties from the pseudo-2D axial-radial simulation, the 1D axial simulations with and without a wall-collision model, and the 2D hybrid simulation of Ref. [31]. The results shown are the average over the entire simulation time, which amounts to one oscillation cycle (rise and drop) of the discharge current. In this regard, since the primary purpose here has been to assess the capability of the single-region pseudo-2D PIC scheme to self-consistently introduce the overall wall-interactions' effect into the simulation in comparison with 1D simulations, we deemed simulating only a single current oscillation cycle sufficient to obtain representative results for such a comparative analysis.

Looking at the plots in Fig. 11, and comparing the predictions of the pseudo-2D simulation against those from the 1D axial simulations and the full-2D reference case, it is observed that, because the pseudo-2D scheme resolves the walls' sheath and the SEE

Table 2 Summary of the numerical and physical parameters used for the pseudo-2D axial-radial simulations

Parameter	Value [unit]
Computational Parameters	
Time step (Δt)	2×10^{-12}[s]
Total simulation time (t_{final})	30×10^{-6}[s]
Axial domain length (L_x)	3.0 [cm]
Radial domain length (L_y)	1.5 [cm]
Cell size ($\Delta x = \Delta y$)	2×10^{-3}[cm]
Initial number of macroparticles per cell for axial grid (N_{ppc_x})	35
Initial number of macroparticles per cell for radial grid (N_{ppc_y})	65
Physical Parameters	
Initial plasma density ($n_{p,init}$)	1×10^{17}[m^{-3}]
Initial neutral gas density at the anode ($n_{n,init}$)	3.22×10^{19}[m^{-3}]
Electron injection temperature (T_e)	10.0 [eV]
Ion injection temperature (T_i)	0.5 [eV]
Anode temperature (T_{anode})	750 [K]
Wall temperature (T_{wall}) [*for pseudo-2D simulation*]	850 [K]
Ad-hoc Bohm mobility coefficient inside the channel ($\boldsymbol{\alpha}_{ch}$)	0.035
Ad-hoc Bohm mobility coefficient in near-plume ($\boldsymbol{\alpha}_{pl}$)	5.0
Ad-hoc wall collision frequency coefficient ($\boldsymbol{\alpha}_w$) [*for 1D axial simulation*]	0.1

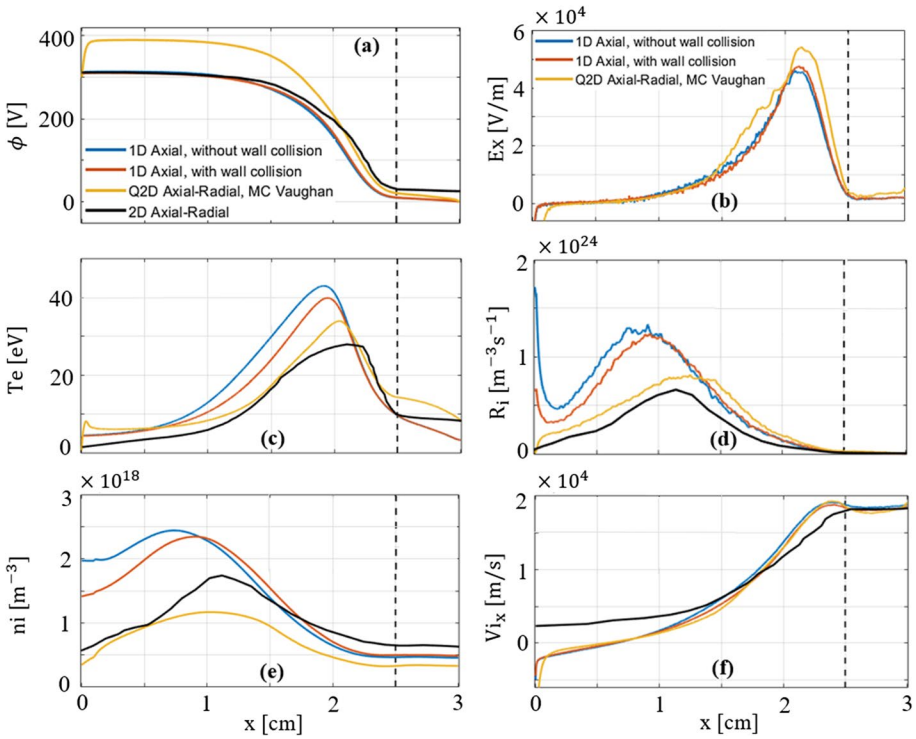

Fig. 11 Time-averaged plasma properties over 30 μs for simulations with different treatments of the wall effects: (**a**) electric potential, (**b**) axial electric field, (**c**) electron temperature, (**d**) ionization rate, (**e**) ions' number density, and (**f**) ions' axial drift velocity. The data for the 2D axial-radial simulation's results are from Ref. [31]. The dashed black line corresponds to the channel exit plane

self-consistently, its predictions in terms of the electron temperature (Fig. 11(c)), the ionization rate (Fig. 11(d)), and the ion number density (Fig. 11(e)) are more consistent with the 2D results compared to the 1D axial simulations (which for instance show a notable ionization rate near the anode).

Therefore, it is logical to say that, with respect to the simulations with ad-hoc wall-collision model, the single-region pseudo-2D simulation can capture more accurately the effect of the channel walls in moderating the electrons' energy, which, in turn, leads to an improved prediction of the processes governed by the electrons' energy distribution, such as the ionization.

Nevertheless, from the plots (a) and (b) in Fig. 11, we can notice the limited applicability of the single-region implementation to simulate the axial-radial coordinates of the thruster. In this respect, it is observed that an unrealistic anode sheath with high potential drop is formed and, consequently, the axial electric field is also overpredicted compared to the 1D simulations. Of course, this feature highlights that the single-region implementation does not provide a very good representation of the Hall thruster domain in the axial-radial configuration due to the strong variations in the sheath properties and the associated wall interactions that exist along the axial direction in a Hall thruster.

In this regard, we recall that the single-region implementation in the axial-radial coordinates implies that the bulk plasma conditions in the radial direction, which in part determine the wall-induced mobility, are an average over the entire axial extent of the

domain. Accordingly, in the near-anode zone, the wall-induced electron mobility is overpredicted, which in turn results in an overprediction of the anode sheath potential drop.

To elaborate on the electrons' axial transport as resolved by the single-region pseudo-2D simulation, we show in Fig. 12 the axial profile of the electrons' drift velocity from the pseudo-2D and the 1D simulations (Fig. 12(a)), alongside the radial distribution of the electron's axial drift velocity from the pseudo-2D simulation (Fig. 12(b)). Figure 12(c) and (d) are the zoomed-in views on the electrons' axial drift velocity plot in the near-anode zone and in the rest of the simulation domain, respectively.

From Fig. 12(b), it is observed that, near the walls in the pseudo-2D simulation, the axial drift velocity of the electrons' population is largely negative, i.e., toward the anode. Moreover, a characteristic oscillation in the axial electrons' velocity has appeared along the radial direction, which is reported in the literature to be the consequence of the Near-Wall Conductivity phenomenon [33], a mechanism that is demonstrated to play a role in enhancing electrons' cross-field transport [2]. Consequently, it is seen in Fig. 12(d) that, in majority of the domain, the axial electrons' drift velocity from the pseudo-2D simulation is more negative compared to the 1D axial simulations in which the effect of the wall interactions on the electrons' mobility is either not captured or incorporated using an ad-hoc model. In addition, from Fig. 12(c), it is observed that the electrons' axial velocity near the anode is significantly more negative in the pseudo-2D case than in the 1D axial simulations. It is as a result of this higher electron axial mobility in the near-anode zone that the anode sheath potential drop in the single-region simulation has increased to hinder further electrons' loss to the anode, while accelerating the ions to ensure an equal flux of particles entering the sheath.

Another interesting observation that we elaborate on in the following is related to the axial distribution of the ions' axial drift velocity, shown in Fig. 11(f). It is observed in this plot that, despite a larger potential drop in the pseudo-2D simulation, the ions'

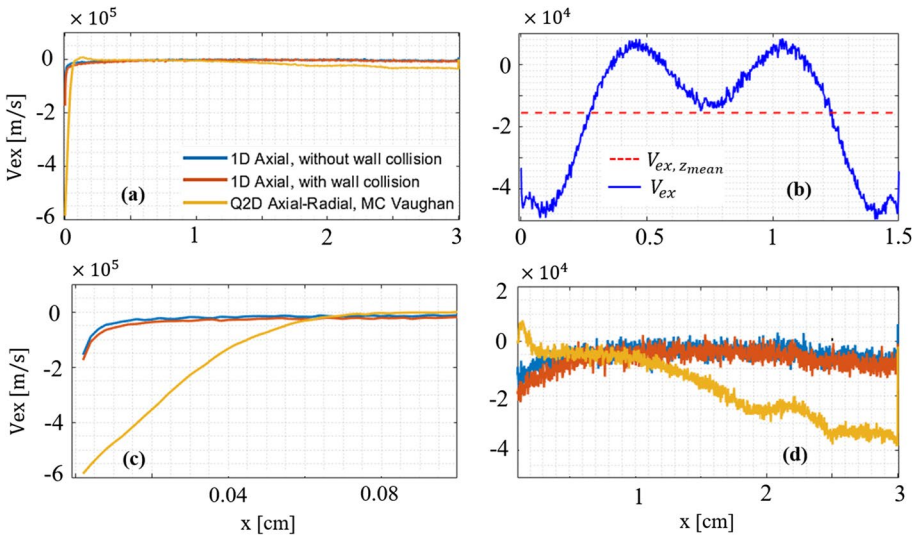

Fig. 12 Distribution of the electrons' axial drift velocity from the pseudo-2D and 1D axial simulations along (**a**) axial direction and (**b**) radial coordinate. Zoomed-in views on plot (**a**) in the near-anode zone and in the rest of the simulation domain are shown in (**c**) and (**d**), respectively

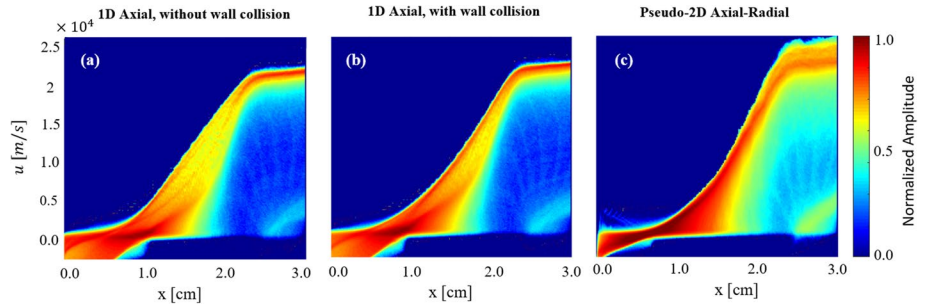

Fig. 13 1D1V ions' velocity distribution function in the $x - u$ coordinates from (**a**) 1D axial simulation with no wall effects, (**b**) 1D axial simulation with ad-hoc wall collision model, and (**c**) pseudo-2D axial-radial simulation

axial drift velocity at the cathode side of the domain is seen to be very close between the pseudo-2D and the 1D axial simulations. This is justified by referring to Fig. 11(c) showing the axial distribution of the ionization rate and Fig. 13, in which the ions' velocity phase plots in the $x - u$ plane is shown with u representing the ions' axial velocity. It is observed in Fig. 11(c) that, compared to the 1D axial simulations, the ionization rate profile in the pseudo-2D simulation shows a downstream shift and is relatively broader in extent. This implies that the ions are also created within the acceleration zone, where most of the acceleration occurs, and, hence, not all ion particles feel the entire potential drop. This, as it can be seen in Fig. 13(c), translates into a higher velocity dispersion in the ions' population in the pseudo-2D simulation with respect to the 1D simulations (Fig. 13(a) and (b)). Accordingly, even though part of the ions' population has indeed reached higher axial velocities in the pseudo-2D case due to the larger potential drop, the larger population of slow ions has caused the mean ion drift velocity from the pseudo-2D simulation to be similar to that from the 1D simulations.

The results and observations discussed above underline that the pseudo-2D PIC simulation has overall the potential to serve as a viable solution to resolve the couplings between the axial and radial phenomena.

In this regard, it is worth highlighting that increasing the number of vertical regions along the axis in the pseudo-2D axial-radial simulations, an effort that has been left for the future work, can allow us to resolve the influence of the axial distributions of the plasma properties on the wall-induced mobility and the SEE. Such multi-region pseudo-2D simulation can enable us to obtain a more accurate picture of the underlying physics, particularly in the context of the discussions in this section regarding the near-anode sheath formation.

Conclusions

In the present article, motivated by the remarkable results that we had obtained from the pseudo-2D PIC scheme in our previous publication [10], we investigated the capabilities of this novel approach in two respects: (1) resolving the coupling between the plasma processes along the different coordinates in a Hall thruster, and (2) incorporating self-consistently in a PIC simulation the average effect(s) of the azimuthal instabilities or plasma-wall interactions on the axial plasma dynamics.

Overall, we demonstrated that, on the one hand, the pseudo-2D PIC scheme can capture the multi-dimensional plasma phenomena in all 2D configurations relevant to a Hall thruster, i.e., axial-azimuthal, azimuthal-radial, and axial-radial. The predictions of the pseudo-2D scheme concerning these phenomena and their coupling were found to be closely similar to those from full-2D reference simulations. On the other hand, we showed that the single-region implementation of the pseudo-2D PIC indeed provides an effective, self-consistent way to resolve the average effects of the azimuthal and radial mechanisms on enhancing electrons' axial mobility and moderating their energy, obviating the need to introduce ad-hoc models of these processes in the PIC simulations.

Starting with the pseudo-2D results in the axial-azimuthal coordinates, we showed that the single-region pseudo-2D simulation can self-consistently resolve the necessary instability-induced electron transport, which, in turn, yields a prediction of the time-averaged plasma properties that is quite similar to the 2D simulation's predictions. In this regard, it was specified that the overall electrons' mobility, as represented by the magnetic force term, was noticed to closely resemble the 2D simulation's result. Moreover, the dispersion characteristics of the captured fluctuations in the azimuthal electric field were shown to be consistent with the theoretical dispersion relation of the ion acoustic waves. This observation emphasizes that the single-region pseudo-2D simulation provides an average representation of the azimuthal physical processes that is, nonetheless, in line with the available literature.

Concerning the ability of the pseudo-2D scheme to capture the interactions in the azimuthal-radial coordinates, we presented some results from the verification simulations we had performed on the plasma-wall interactions in the IPPL code to demonstrate that the baseline PIC code provides an accurate picture of the sheath formation in the presence of the Secondary Electron Emission. Next, comparing the results from the pseudo-2D simulations vs a 1D radial and a 1D azimuthal simulation, we observed that the pseudo-2D approach is remarkably able to predict some of the main interactions and couplings reported in the literature between the azimuthal and radial processes; namely, the change in the sheath evolution in the presence of the azimuthal waves, the sheath transition to the space-charge saturated limit, and the consequent Near-Wall Conductivity. Furthermore, it was shown that the influence of the wall physics on the dynamics of the azimuthal instabilities and the associated wave-induced electrons' mobility is also captured by the single-region pseudo-2D simulation. These results confirm the great potential of the pseudo-2D PIC, even in its single-region implementation, to resolve the complex, multi-dimensional behavior of the plasma phenomena in the azimuthal-radial coordinates, a capability that so far has been exclusive to computationally expensive 2D simulations.

Finally, in the axial-radial coordinates, we demonstrated that the single-region pseudo-2D simulation captures self-consistently the average effect of the wall collisions and the SEE phenomenon on the electrons' dynamics, which affect the global plasma behavior. Accordingly, the pseudo-2D simulation was seen to provide an improved prediction of the time-averaged plasma properties' distribution with respect to a 1D axial simulation with ad-hoc wall-collision model such that the pseudo-2D results were more consistent with the results of the 2D reference simulation. In addition, we observed that the influence of the bulk-plasma conditions on the near-wall sheath processes was also captured

in the pseudo-2D simulation. Indeed, we illustrated that the overestimation of the anode sheath potential drop due to an overpredicted electrons' axial mobility in the near-anode zone was the physical consequence of the single-region implementation that resolves the radial physics based on an axially averaged bulk-plasma conditions. This is a testament to the fact that the pseudo-2D PIC is, in principle, able to capture the coupling between the radial and axial processes in a physically consistent way but that its single-region implementation may not be the best choice to resolve this coupling.

In this regard, it is recalled that the decision to focus on single-region pseudo-2D PIC simulations in this effort was driven by the objectives of the research and also the fact that this implementation provides the maximum reduction in the computational cost. As such, we aimed at thoroughly testing the capabilities of the single-region approach in this paper. Nevertheless, we underline that the single-region implementation of the pseudo-2D PIC scheme can be only valid for rather simple geometries and for problems that can be actually described through the single decomposition of the problem. In our previous work [10], we showed that, in the axial-azimuthal coordinates, increasing the number of vertical regions to two, i.e., the so-called "double-region" implementation [10], can improve the predictions of plasma properties as it provides the simulation with the necessary degree of freedom to resolve the axial variation in the azimuthal waves' characteristics. Accordingly, a similar improvement can also be logically expected in the axial-radial coordinates and the azimuthal-radial coordinates if we increase the number of vertical, but also horizontal, regions.

Before doing so, however, we decided to, first, further generalize the pseudo-2D PIC scheme by strengthening its underpinning formulation, which currently lacks a rigorous mathematical framework. This activity is almost concluded, and the outcomes will be presented in a follow-up publication. However, the results and discussions in this paper reaffirm that the pseudo-2D scheme provides a strong foundation to proceed to a reduced-order PIC scheme, which incorporates a mature formulation for the decomposition of Poisson's equation. In this respect, based on the fascinating capabilities observed for the pseudo-2D PIC scheme to resolve the multi-dimensional plasma processes, the reduced-order PIC can serve as a breakthrough in the kinetic plasma modeling and, particularly in our context, toward enabling computationally efficient 3D PIC simulations of Hall thrusters.

Appendix

Plasma-wall interactions module in the IPPL PIC code

The wall interactions module consists of functions that govern the treatment of particles colliding with the boundary surfaces of the simulation domain. It comprises various reflection algorithms (isotropic, diffuse, or specular) for particles hitting the surface, a subroutine for recombination of ions on the surface, and different models for handling Secondary Electron Emission from the walls that were briefly introduced in IPPL particle-in-cell code and the pseudo-2D PIC scheme. For each of these functionalities, we have performed dedicated verifications against well-established cases from the literature. In particular, the implementation of the Monte-Carlo-based Vaughan model for the SEE has been verified using the mini-benchmark suggested in Ref. [34]. Moreover, we validated the wall interactions module against the well-known simulation case of

Schwager and Birdsall that corresponds to the classic formation of a "collector" sheath in the presence of a source plane [35].

In this section, we present the results of a 1D radial simulation we performed to verify the plasma-wall interactions module in a setting representative of a Hall thruster. This simulation is inspired from Ref. [14], in which the authors extended the source-collector sheath problem of Schwager and Birdsall [35] to simulate a domain representing half of the radial extent of a Hall thruster, from the bulk-plasma to the wall, with the plasma properties at the bulk (source plane) corresponding to the typical values encountered in the near-anode, ionization, and acceleration zone of a Hall thruster domain. For our simulations below, the bulk plasma conditions are representative of the acceleration region (Table 3).

To briefly summarize the simulation conditions, the electrons and ions are sampled from a half-Maxwellian distribution at the temperatures reported in Table 1 and are injected into an initially empty domain at the source plane. The source plane corresponds to the sheath edge, where the plasma can be considered quasi-neutral. Therefore, to maintain quasi-neutrality at the source plane, the approach reported in Ref. [14] is pursued. The electrically floating boundary condition [36] is applied to the surface facing the plasma particles. The constant SEE yield model is used for these simulations. Other aspects of the simulation's setup are similar to those in Ref. [14].

Figure 14 presents the variation in the sheath potential drop and the density distribution of plasma particles for four different constant values of the SEE coefficient. The wall potential in each of the simulation cases is compared against the theoretical near-wall sheath potential drop ($\Delta\phi_s$) as given by Eq. 15 [14]. In this equation, $T_{e\|}$ is the electron temperature component in the direction parallel to the magnetic field, calculated in the quasi-flat region after the source sheath to obtain the values of the potential drop shown in Fig. 14(b). In addition, γ_{SEE} is the electron emission yield coefficient, and m_e and m_i are, respectively, the electron and ion mass.

$$\Delta\phi_s = T_{e||}\ln\left((1-\gamma_{SEE})\sqrt{\frac{m_i}{2\pi m_e}}\right). \tag{15}$$

Table 3 Input data for the wall-interactions module verification simulation; the properties are representative of the values encountered in the acceleration region of a standard Hall thruster

Parameter	Value [unit]
Neutral density	$2 \times 10^{18}[m^{-3}]$
Plasma density	$3 \times 10^{17}[m^{-3}]$
Plasma potential	200 [V]
Radial magnetic field	0.015 [T]
Axial magnetic field	0 [T]
Axial electric field	10,000 [V/m]
Electron temperature	20 [eV]
Ion temperature	0.15 [eV]
Neutral temperature	700 [K]

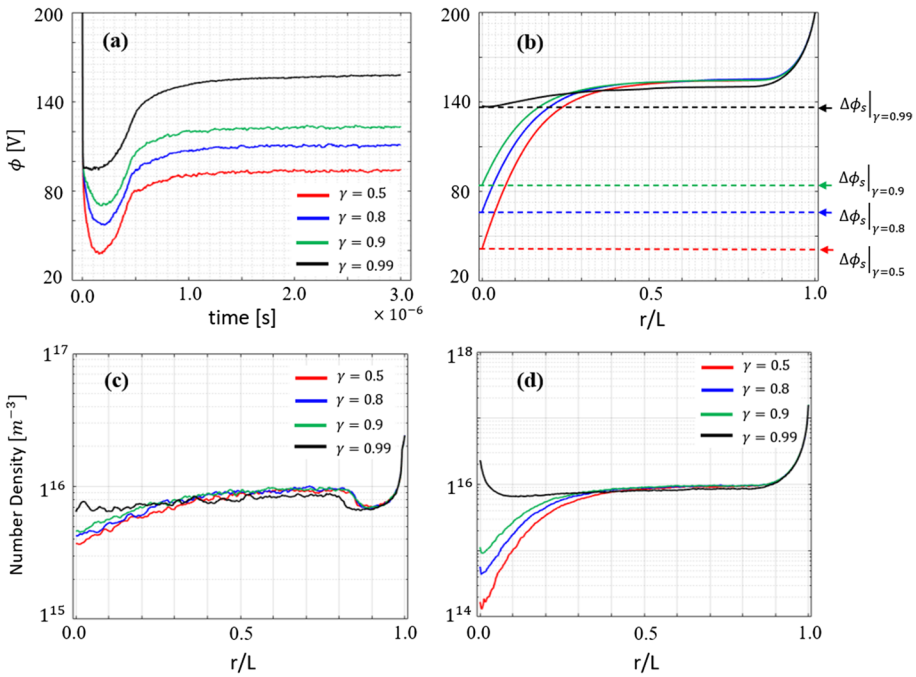

Fig. 14 Sheath behaviour in the presence of various levels of SEE; (**a**) time evolution of the wall potential, (**b**) plasma potential distribution, (**c**) ion density distribution, (**d**) electron density distribution. The x-axis in plots (**b**)-(**d**) is normalized with respect to the simulation domain's length

As it is seen in Fig. 14(a), the simulations have reached steady state after about 2 μs. Furthermore, in the plots (b)-(d) in Fig. 14, it is observed that, as the SEE yield coefficient increases, the sheath potential drop decreases while the near-wall electron density increases. Eventually, when γ_{SEE} becomes larger than the critical value for xenon of 0.983 (the assumed propellant in these simulations), the sheath potential becomes almost flat near the wall, and accordingly, the ion density remains constant whereas the electron density increases sharply. These are evidence that the sheath is in the space-charge saturated limit as expected from the theory.

Besides the above observations, it is underlined that the simulated sheath potential drops for all values of SEE yield agree well with the corresponding theoretical values (Fig. 14(b)), confirming the validity of the simulation results and, hence, the implementation details of the wall-interactions module in our PIC code.

Sensitivity of the single-region axial-azimuthal simulation to the initial number of macroparticles per cell

As it was mentioned in Simulation setup section for the axial-azimuthal simulations the single-region pseudo-2D axial-azimuthal simulation, whose results were presented in Results and discussion section was carried out with a nominal initial macroparticles per cell of 300 along the azimuthal direction. In this section of the appendix, we present the single-region pseudo-2D simulation results for various initial numbers of macroparticles per cell ($N_{ppc,init}$). The $N_{ppc,init}$ is varied from 75 to 1200 particles, and the simulation

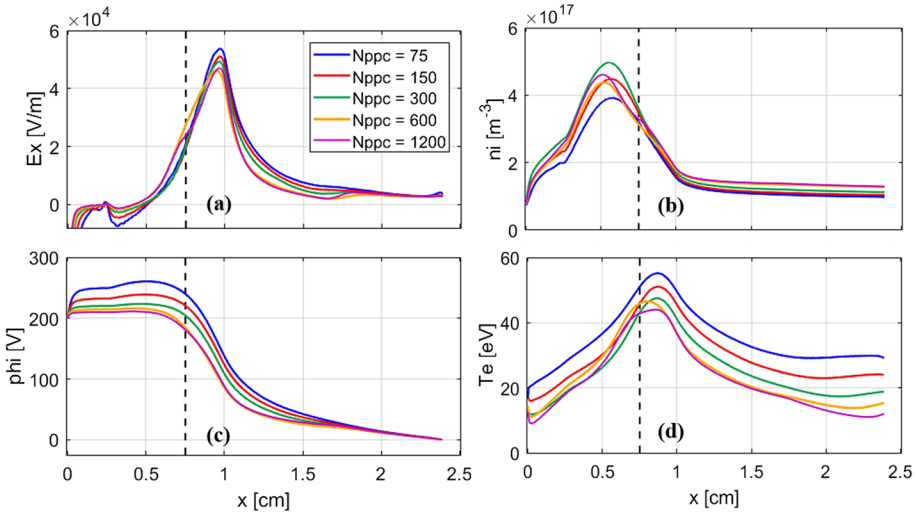

Fig. 15 Single-region pseudo-2D simulation results in the axial-azimuthal configuration for various numbers of initial macroparticles per cell; (**a**) electric field, (**b**) ion number density, (**c**) plasma potential, (**d**) electron temperature

results in terms of the axial distribution of the time-averaged plasma properties, electric field (E_x), ion number density (n_i), plasma potential (ϕ), and electron temperature (T_e) are shown in Fig. 15.

Referring to the plots in Fig. 15, it is clear that, from 300 macroparticles per cell, the variation in the plasma properties' profiles is rather minor, with the simulation cases with $N_{ppc,init}$ of 600 and 1200 almost providing identical results. Moreover, increasing the macroparticles per cell from 75 to 1200, the inflation in the near-anode plasma potential (Fig. 15(c)) is seen to reduce, resulting in lower peaks of the electric field (Fig. 15(a)). Regarding the electron temperature (Fig. 15(d)), by increasing the number of macroparticles per cell, the peak electron temperature and its values near the anode and cathode boundaries are observed to decrease. Finally, referring to Fig. 15(b), a non-monotonic behavior is observed with respect to ion number density when going from 75 to 1200 macroparticles per cell. Indeed, increasing $N_{ppc,init}$ from 75 to 300, the peak ion number density is seen to increase whereas, from 300 macroparticles per cell to 600, the ion number density peak slightly decreases and then remains almost constant.

Overall, it is possible to conclude that, even though the pseudo-2D scheme is sensitive to the number of macroparticles per cell along the azimuthal direction, it shows a moderate sensitivity to this parameter, especially for $N_{ppc,init}$ values above 300.

Authors' contributions

All authors contributed to the conception of this study. Material preparation, data collection and analysis were performed by Maryam Reza and Farbod Faraji. The first draft of the manuscript was written equally by Maryam Reza and Farbod Faraji. Aaron Knoll supervised the research and reviewed the draft manuscript. All authors read and approved the final revised manuscript for submission.

Funding

The present research is carried out within the framework of the project "Advanced Space Propulsion for Innovative Realization of space Exploration (ASPIRE)". ASPIRE has received funding from the European Union's Horizon 2020 Research and Innovation Programme under the Grant Agreement No. 101004366. The views expressed herein can in no way be taken as to reflect an official opinion of the Commission of the European Union.

Availability of data and materials
The datasets supporting this study are available from the corresponding author on reasonable request.

Declarations

Competing interests
The authors have no competing interests to declare that are relevant to the content of this article.

Received: 25 May 2022 Accepted: 25 September 2022
Published online: 14 October 2022

References

1. Kaganovich ID et al (2020) Physics of E × B discharges relevant to plasma propulsion and similar technologies. Phys Plasmas 27:120601
2. Boeuf JP (2017) Tutorial: Physics and modeling of Hall thrusters. J Appl Phys 121:011101
3. Taccogna F, Garrigues L (2019) Latest progress in Hall thrusters plasma modelling. Rev Mod Plasma Phys 3:12. https://doi.org/10.1007/s41614-019-0033-1
4. Sekerak MJ, Plasma Oscillations and Operational Modes in Hall Effect Thrusters, PhD Dissertation (2014)
5. Heron A, Adam JC (2013) Anomalous conductivity in Hall thrusters: Effects of the non-linear coupling of the electron-cyclotron drift instability with secondary electron emission of the walls. Phys of Plasmas 20:082313
6. Coche P, Garrigues L (2014) A two-dimensional (azimuthal-axial) particle-in-cell model of a Hall thruster. Phys Plasmas 21:023503
7. Charoy T et al (2021) The interaction between ion transit-time and electron drift instabilities and their effect on anomalous electron transport in Hall thrusters. Plasma Sources Sci Technol 30:065017
8. Lafleur T, Chabert P (2018) The role of instability-enhanced friction on "anomalous" electron and ion transport in Hall-effect thrusters. Plasma Sources Sci Technol 27:015003
9. Mikellides IG and Ortega AL (2021) Growth of the lower hybrid drift instability in the plume of a magnetically shielded Hall thruster. J Appl Phys 129;193301
10. Faraji F, Reza M, Knoll A (2022) Enhancing one-dimensional particle-in-cell simulations to self-consistently resolve instability-induced electron transport in Hall thrusters. J Appl Phys 131:193302
11. Garrigues L, Tezenas du Montcel B, Fubiani G et al. Application of sparse grid combination techniques to low temperature plasmas particle-in-cell simulations I Capacitively coupled radio frequency discharges. J Appl Phys. (2021);129:153303
12. Turner M.M et al. Simulation benchmarks for low-pressure plasmas: Capacitive discharges. Phys Plasmas (2013);20:013507
13. Lafleur T, Baalrud SD, Chabert P (2016) Theory for the anomalous electron transport in Hall effect thrusters. I. Insights from particle-in-cell simulations. Phys Plasmas 23:053502
14. Taccogna F, Longo S, Capitelli M (2005) Plasma sheaths in hall discharges. Phys Plasmas 12:093506
15. Bezanson J, Edelman A, Karpinski S, Shah VB (2017) Julia: A fresh approach to numerical computing. SIAM Rev 59:65–98
16. Blackman D, Vigna S (2021) Scrambled linear pseudorandom number generators. ACM Trans Math Softw 47:1–32
17. Vahedi V, Surendra M (1995) A Monte Carlo collision model for the particle-in-cell method: applications to argon and oxygen discharges. Comput Phys Commun 87:179–198
18. Carbone E, Graef W, Hagelaar G et al (2021) Data Needs for Modeling Low-Temperature Non-Equilibrium Plasmas: The LXCat Project, History, Perspectives and a Tutorial. Atoms 9(1):16
19. Biagi-v7.1 database, www.lxcat.net, retrieved on May 15, 2021.
20. Croes V, "Modélisation bidimensionnelle de la décharge plasma dans un propulseur de Hall". Université Paris Saclay (COmUE). Français. ⟨tel-01652098v2⟩ (2017)
21. Vaughan J (1989) A new formula for secondary emission yield. IEEE Trans on Electron Devices 36:9
22. Box GEP, Muller ME (1958) A Note on the generation of random normal deviates. Ann Math Stat 29(2):610-611
23. Boris JP, The acceleration calculation from a scalar potential. Plasma Phys Lab Princeton Univ MATT-152(1970)
24. Charoy T et al (2019) 2D axial-azimuthal particle-in-cell benchmark for low-temperature partially magnetized plasmas. Plasma Sources Sci Technol 28:105010
25. Charoy T, Numerical study of electron transport in Hall thrusters. Plasma Physics [physics.plasm-ph], Institut Polytechnique de Paris. English. ⟨NNT: 2020IPPAX046⟩ ⟨tel-02982367⟩ (2020)
26. Reza M, Faraji F, Andreussi T, Andrenucci M. A Model for Turbulence-Induced Electron Transport in Hall Thrusters. IEPC-2017–367, 35th International Electric Propulsion Conference, Atlanta, Georgia (2017)
27. Faraji F, Reza M, Andreussi T, "Modular Comprehensive Modeling of Plasma Behavior in Hall Thrusters", IEPC-2019–147. 36th International Electric Propulsion Conference. Vienna (2019)
28. Boeuf JP, Garrigues L (2018) E × B electron drift instability in Hall thrusters: Particle-in-cell simulations vs. theory. Phys Plasmas 25:061204
29. Charoy T, Bourdon A, Chabert P, Lafleur T, Tavant A, "Oscillation analysis in Hall thrusters with 2D (axial-azimuthal) Particle-In-Cell simulations", IEPC-2019-A487.36th International Electric Propulsion Conference, Vienna (2019)
30. Villafana W et al (2021) 2D radial-azimuthal particle-in-cell benchmark for E×B discharges. Plasma Sources Sci Technol 30:075002

31. Panelli M. et al. Axisymmetric Hybrid Plasma Model for Hall Effect Thrusters. Particles, 4 (2021)
32. Hagelaar GJM, Bareilles J, Garrigues L, Boeuf JP (2002) Two-dimensional model of a stationary plasma thruster. J Appl Phys 91:5592
33. Domínguez-Vázquez A, Taccogna F, Ahedo E (2018) Particle modeling of radial electron dynamics in a controlled discharge on a Hall thruster. Plasma Sources Sci Technol 27:064006
34. Sydorenko D. Particle-in-Cell Simulations of Electron Dynamics in Low Pressure Discharges with Magnetic Fields. PhD Dissertation, (2006)
35. Schwager LA, Birdsall CK (1990) Collector and source sheaths of a finite ion temperature plasma. Phys Fluids B 2:1057
36. Verboncoeur JP, Alves MV, Vahedi V. Simultaneous Potential and Circuit Solution for Bounded Plasma Particle Simulation Codes. EECS Department, UC Berkley, Memorandum No. UCB/ERL M90/67 (1990)